SAND2010-8732C

Proceedings of the ASME/JSME 2011 8th Thermal Engineering Joint Conference
AJTEC2011
March 13-17, 2011, Honolulu, Hawaii, USA

AJTEC2011-44097

RAMAN AND INFRARED THERMOMETRY FOR MICROSYSTEMS

Leslie M. Phinney[1], Wei-Yang Lu[2], and Justin R. Serrano[1]
Sandia National Laboratories*
[1]Albuquerque, New Mexico, USA and [2]Livermore, California, USA

ABSTRACT

This paper compares measurements made by Raman and infrared thermometry on a SOI (silicon on insulator) bent-beam thermal microactuator. Both techniques are noncontact and used to experimentally measure temperatures along the legs and on the shuttle of the thermal microactuators. Raman thermometry offers micron spatial resolution and measurement uncertainties of ±10 K; however, typical data collection times are a minute per location leading to measurement times on the order of hours for a complete temperature profile. Infrared thermometry obtains a full-field measurement so the data collection time is much shorter; however, the spatial resolution is lower and calibrating the system for quantitative measurements is challenging. By obtaining thermal profiles on the same SOI thermal microactuator, the relative strengths and weaknesses of the two techniques are assessed.

INTRODUCTION

High spatial resolution thermal metrology is necessary for assessing thermal gradients across microsystems devices. Direct thermal measurements are used to further understanding of microelectromechanical systems (MEMS) device performance, validate simulations, and optimize designs [1]. Optical temperature measurement techniques are non-contact and commonly used to determine the temperatures of microsystems components. Methods have been developed based on a variety of thermophysical phenomena including thermoreflectance, pyrometry, fluorescence, interferometry, scanning thermal microscopy, infrared imaging, and Raman spectroscopy [2-4]. Typically, temperature measurements are made by one of these techniques and reported in the literature. Measurements by multiple techniques on the same microdevice are less common. Temperature measurements have been previously reported for thermal microactuators using resistance thermometry [5], scanning probe thermometry [6], Raman spectroscopy [7, 9], and infrared imaging [10].

Thermal microactuators are enabling components in many MEMS designs including optical switches [11, 12] and nanopositioners [13]. Their advantages include higher force generation, lower operating voltages, and less susceptibility to adhesion failures compared to electrostatic microactuators. However, thermal microactuators have higher power requirements than electrostatic microactuators, and their switching speeds are limited by their cooling time. Multiple thermal microactuator designs have been demonstrated including symmetric designs fabricated from a single material that have been referred to as bent-beam, chevron, or V-shaped actuators. These types of microactuators have angled legs that expand when Joule-heated by an electrical current, providing force and displacement output. Extensive work has been performed designing, fabricating, testing, and modeling bent-beam MEMS thermal actuators fabricated using surface micromachining [5-7, 14-17] and single crystal silicon processing [6, 10-13].

This study was undertaken to advance the understanding of thermometry for microsystems by comparing temperature measurements on bent-beam microactuators using Raman and infrared thermometry. The thermal microactuator design and fabrication is described. The experimental methods for Raman and infrared thermometry are then reviewed. The measured data are then reported followed by conclusions.

Table 1: Thermal Microactuator Leg Dimensions from Anchor to Shuttle

* This manuscript has been authored by Sandia Corporation under Contract No. DE-AC04-94AL85000 with the U.S. Department of Energy. The United States Government retains and the publisher, by accepting the article for publication, acknowledges that the United States Government retains a non-exclusive, paid-up, irrevocable, world-wide license to publish or reproduce the published form of this manuscript, or allow others to do so, for United States Government purposes.

TMA	Length (µm)	Width (µm)	Thickness (µm)
1	7000	65	125
2	5500	50	125
3	5500	85	125

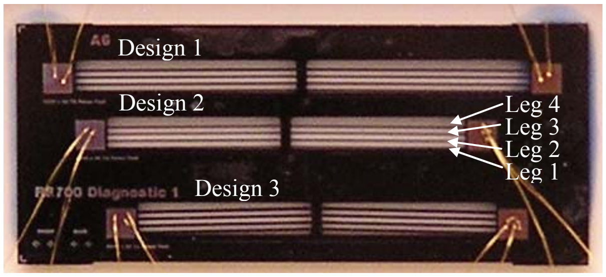

Figure 1: Picture of SOI thermal microactuators. The thermal microactuators are numbered 1, 2, and 3 from top to bottom. The microactuator legs are numbered 1, 2, 3, and 4 from bottom to top. Two wires bonded to each bond pad are visible in the image. The square bond pads are 900 µm x 900 µm. The connections to the package are outside of the image.

THERMAL MICROACTUATOR DESIGN AND FABRICATION

In SOI (silicon on insulator) MEMS fabrication, the initial wafer has three layers: a single crystal silicon substrate wafer, a thermally grown silicon dioxide layer referred to as the buried oxide, and a mechanically thinned single crystal silicon layer called the device layer. A DRIE (deep reactive ion etching) process enables high-aspect ratio, deep etching of features in silicon wafers using a three step process of conformal polymer deposition, ion sputtering, and chemical etching of the Si. DRIE can be performed on both the device and substrate layers in order to pattern thermal microactuators from the device layer and remove the substrate underneath the microactuators [18] to reduce heat loss and required power during operation [1]. A 0.7 µm layer of aluminum is deposited on top of the device layer to improve electrical connections when the parts are packaged.

The SOI thermal microactuators (TMA) were fabricated from a wafer with: a 550 µm thick substrate, a 2 µm buried oxide layer, and a 125 µm thick device layer. Three thermal microactuators were fabricated with actuator leg lengths from the anchor to the shuttle, widths, and thicknesses listed in Table 1. The measurements presented in this paper were made on a thermal microactuator design 2 in Table 1 that has legs 5500 µm long from the anchor to the shuttle, 50 µm wide, and 125 µm thick. During packaging, wires are bonded to the 0.7 µm aluminum layer that is deposited on top of the bond pad. Figure 1 shows a packaged die with the three thermal microactuators and bond wires visible. The thermal microactuator designs and legs on design 2 are numbered.

RAMAN THERMOMETRY

Temperature measurements were obtained with micro-Raman spectroscopy [7-8] using a Renishaw inVia Raman microscope. The microscope uses a 180° backscattering geometry and a 488 nm Ar+ laser as the probe that produces a diffraction-limited spot of 560 nm in diameter when focused by a 50×, 0.50-numerical-aperture objective. The actual measurement diameter within the sample is larger, 1.70 µm, because of spreading of the probe laser within the sample. The Raman signal from the sample surface is collected through the objective, dispersed by a grating spectrograph, and detected with a thermoelectrically cooled CCD camera with a spectral resolution of is 0.95 cm^{-1}/pixel.

In the Raman process, photons from the incident probe light source interact with the optical phonon modes of the irradiated material and are scattered to higher (anti-Stokes) or lower (Stokes) frequencies from the probe line frequency. In the case of silicon and polycrystalline silicon, the scattered Raman light arises from the triply degenerate optical phonon at the Brillouin zone center. The resulting spectrum for the Stokes (lower frequency) Raman response has a single narrow peak at ~520 cm^{-1} from the laser line frequency at room temperature. Increases in temperature affect the frequency, lifetime, and population of the phonon modes coupled to the Raman process, leading to changes in the Raman spectra, namely a shift in the peak position and broadening of the Raman peak. Both metrics are practical for temperature mapping of MEMS. However, while peak width is sensitive only to surface temperature, peak position is sensitive to both stress and temperature [7, 19].

Laser power at the sample is maintained at a level that minimizes localized heating of the sample that would otherwise introduce a bias into the temperature measurement. Minimal heating of the sample is confirmed by obtaining Raman spectra at decreasing laser powers from a room-temperature sample until no change in the Raman peak position was observed. The SOI die were packaged in a ceramic dual in-line package (DIP) which was inserted into a zero insertion force (ZIF) socket, enabling electrical connections to a power supply. The thermal microactuators were powered with a Keithley 2400 Source Meter where the voltage was sourced and power monitored.

Prior to performing the measurements on the test structures, a temperature calibration of the Raman response from a SOI die was obtained by placing a die in a second temperature-controlled hot stage and acquiring Raman data over a temperature range of 300-700 K. A Voight function, which captures both the Lorentzian Raman line shape and the Gaussian instrument function, is fitted to the Raman spectral data to extract the center position, Ω, of the Raman peak [7]. At different temperatures in the calibration range, six spectra are acquired from the sample and fitted, and the extracted peak position is then averaged and plotted as a function of temperature.

The data are then fitted to a calibration function that correlated the observed change in the Raman spectra to temperature. Since the thermal microactuator is free to expand allowing stresses to relax, the peak position can be used for thermometry measurements. For the Raman peak position, the correlation is linear and is described by the expression:

$$\Omega = \frac{\partial \Omega}{\partial T} T + \Omega_o , \tag{1}$$

where $\partial\Omega/\partial T = (-0.0232)$ cm^{-1}/K, T is in K, and $\Omega_o = 527.2$ cm^{-1}. Measurements are made on the unpowered actuator and a reference silicon sample to monitor the Raman instrument and correct for any drift in the system as well as the powered thermal microactuator. Due to the package and socket having a thermal equilibration time of 30 to 45 minutes, the unpowered measurements are made prior to or after voltage is applied to the thermal microactuator. The reference silicon measurements are conducted during the unpowered and powered microactuator measurements. Six spectra are acquired for each data location, and the extracted peak position is averaged and used to calculate the temperature and uncertainty.

INFRARED THERMOMETRY

A Flir A325 infrared camera (IR) system with close-up 1x lens was used to characterize the temperature profiles of the actuator. The IR camera has a resolution of 320x240 pixels. Its microbolometer type of detector receives infrared radiation with wavelengths between 7.5-14 μm heating the detector material and changing its electrical resistance. This resistance change is measured and processed into temperatures which can be used to create an image. The 1x close-up lens provides a field of view (FOV) of 8x6 mm, which corresponds to a resolution of 25 μm/pixel. Both camera control and temperature analysis are from a PC using ExaminIR software. The system was factory calibrated, but it requires input of the emissivity of the object to calculate the temperature. Since few data are available for the single crystal silicon [20], emissivity calibration was performed. It was done by placing an unpackaged die on a hot plate, as shown on Figure 2. A thermocouple (TC) was attached on the top surface of the die. The IR camera was focused on the surface of the die at an area near the thermocouple. Both the thermal image and TC reading were recorded. The procedure was repeated at several discrete temperatures to obtain a calibration curve shown in Figure 3. It shows emissivity $e = 0.8$ is the best value for this investigation.

RESULTS AND DISCUSSION

Figure 4 shows temperature profiles on thermal microactuator design 2 obtained using Raman thermometry along the thermal microactuator legs from the anchor (position-0 μm) to the shuttle (position-5500 μm) at 500 μm increments when powered with 5V or 7V. Due to symmetry, the temperature profiles on the second half of the thermal microactuator are a mirror image of the profiles shown. The open symbols are the data points, and the lines are guides to the eye. When viewed so that the motion occurs in an upward direction, Leg 1 is at the bottom and Leg 4 is at the top as indicated in Fig. 1. As seen in the figure, the middle leg, Leg 3, achieves a higher maximum temperature than the outer legs, Legs 1 and 4. Also, the maximum temperatures along the thermal microactuator legs occur around 3500 μm from the anchor, a little less than two thirds of the distance from the anchor to the shuttle, for both the 5V and 7V cases. The maximum measured temperatures are 437K, 425K, and 415K at 7V and 370K, 364K, and 358K at 5V for Legs 3, 4, and 1, respectively.

When voltage is applied to the thermal microactuator, the entire ceramic DIP package containing the die heats up significantly. A thermocouple was attached to the side of the package to monitor the heating of the package. The temperature of the socket holding the die increases ~3K at 3V, ~5K at 5V, ~10K at 7V, and nearly ~13K at 9V. The overall heating of the die is also reflected in the anchor temperatures, which increase ~20K at 5V and ~30K at 7V as seen in Fig. 4.

Figure 5 contains temperature measurements on thermal microactuator design 2 operated at 5V and 7V obtained using Raman thermometry at -10 μm, 1800 μm, and 3600 μm from edge of the anchor (position = 0 μm) vertically upward in the direction of actuator motion. The locations of the legs are marked on the figure. The open markers are the data points, and the line at -10 μm is to guide the eye. There are no lines connecting the data at 1800 μm and 3600 μm since between the legs there is no connecting material or underlying substrate. The data in Fig. 5 again shows that the center legs, 2 and 3, achieve higher temperatures than the outer legs, 1 and 4.

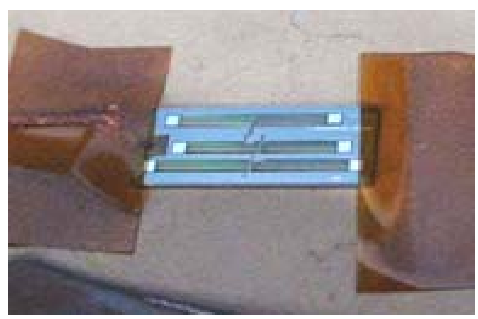

Figure 2: Sample and experimental setup for infrared thermometry.

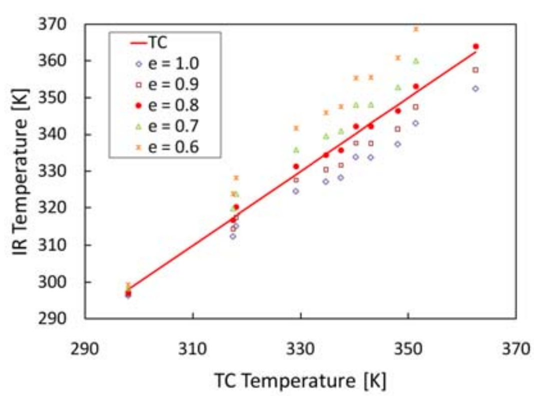

Figure 3: Calibration of infrared thermal imaging system.

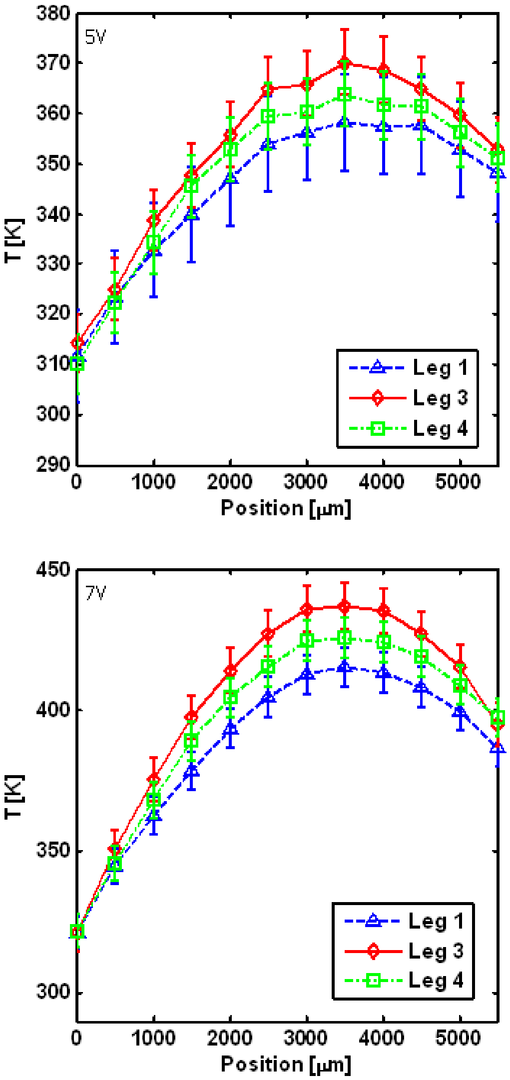

Figure 4: Temperature profiles on thermal microactuator design 2 obtained using Raman thermometry on the thermal microactuator legs from the anchor (position-0 μm) to the shuttle (position-5500 μm) when powered with 5V or 7V. When viewed so that the motion occurs in an upward direction, Leg 1 is at the bottom and Leg 4 is at the top.

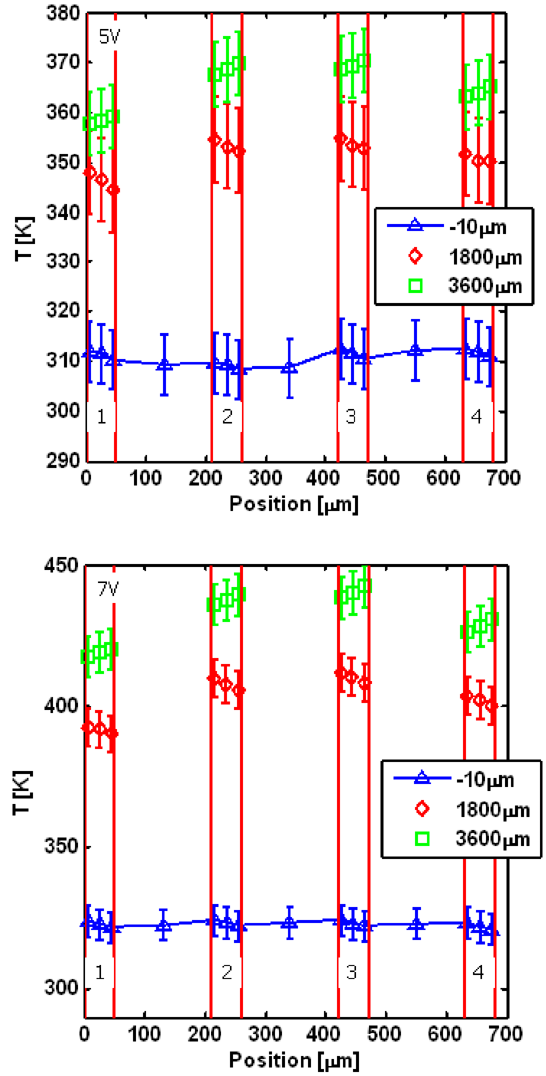

Figure 5: Temperature measurements on thermal microactuator design 2 operated at 5V and 7V obtained using Raman thermometry at -10 μm, 1800 μm, and 3600 μm from edge of the anchor (position-0 μm) vertically upward in the direction of actuator motion. When viewed so that the motion occurs in an upward direction, Leg 1 is at the bottom and Leg 4 is at the top.

Trending observed in the temperatures across each leg is likely stress-induced bias in the temperature measurements since the slope is consistent with the change in stress across a bending beam. Thus, the slight downward trend for points at -10 and 1800 μm, would indicate a slight compressive stress on the top half of the leg and a slight tensile stress on the bottom side. For the points at 3600 μm, the opposite trend is observed with the top in slight tension and the bottom in slight compression. However, in spite of this, given the small magnitude of the differences across the leg and the level of uncertainty which can confidently attribute to the measurement, a fully quantitative determination of stress would be difficult.

Figure 6 depicts Raman temperature measurements made at 3V, 5V, 7V, and 9V along the center of the shuttle of thermal microactuator design 2 taken starting at 20 μm from the rounded end of the shuttle to the opposite end, with measurements every 150 μm. The four leg positions are marked. The open markers are the data points and the lines a guide to the eye. The thermal gradient along the shuttle increases at the higher operating voltages with shuttle staying cooler in the vicinity of Leg 1 since the shuttle protrudes more than 600 μm past the location where Leg 1 extends from the shuttle providing a thermal mass acting to reduce the temperature. This and the smaller gap between the sidewall and Leg 1 than for Leg 4 explain the temperature difference between Leg 1 and Leg 4 observed in the temperature profiles in Fig. 4.

For infrared thermometry measurements, the temperature fields at 3 V, 5 V and 7 V excitation of design 2 are shown in Figure 7. Detailed temperature profiles along the beams and shuttle are plotted in Figures 8 and 9, respectively. The temperatures of two inner beams (Legs 2 and 3) are generally the same and higher than the temperatures of two outside beams (Legs 1 and 4). The hottest region of Leg 2 (or Leg 3) is about 3200 μm from the anchor, which is around 60% of the distance from the anchor to the substrate. The maximum temperature is close to 435 K for 7 V excitation. The uncertainty in the infrared temperature measurements is determined from the calibration data, thermocouple uncertainty, and variation in the silicon surface to be ±10K.

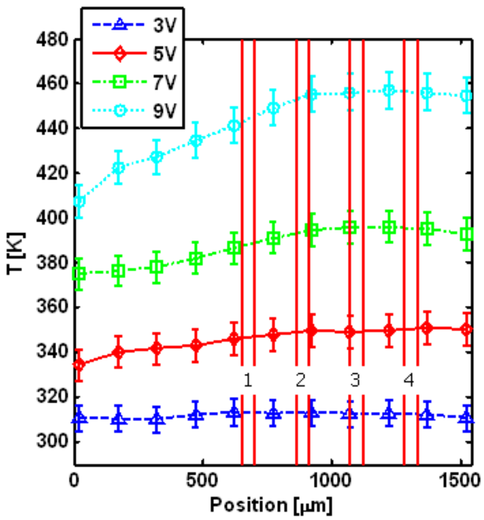

Figure 6: Raman temperature measurements made at 3V, 5V, 7V, and 9 V along the shuttle of thermal microactuator design 2 taken starting at 20 μm from the rounded end of the shuttle to the opposite end, with measurements every 150 μm. The four leg positions are marked.

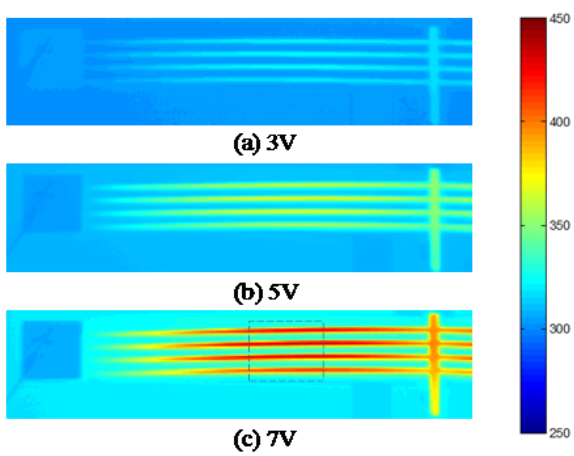

Figure 7: Infrared thermal images of thermal microactuator design 1 at a) 3V, b) 5V, and c) 7V. Temperature profiles in K are shown along the beams from the anchor to the substrate.

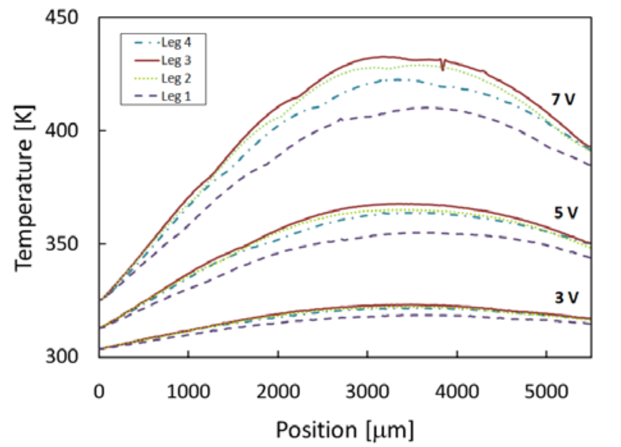

Figure 8: Temperature profiles on thermal microactuator design 2 obtained using infrared thermometry when powered at 3V, 5V, and 7V.

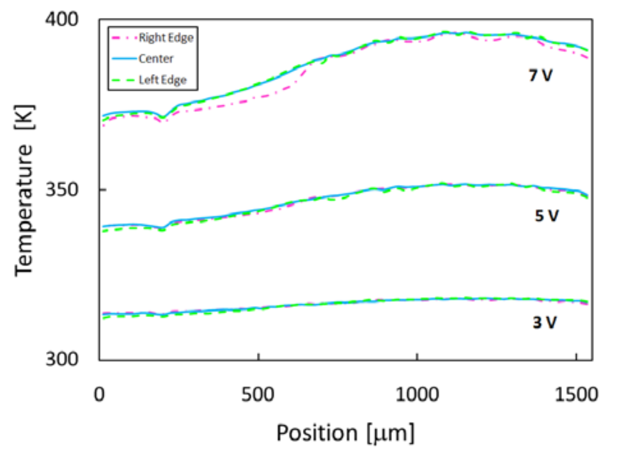

Figure 9: IR temperature measurements made at 3V, 5V, and 7V along the shuttle of thermal microactuator design 2. The dip in temperature observed at ~200 μm corresponds to a metal line patterned on the silicon for which the surface emissivity calibration is incorrect.

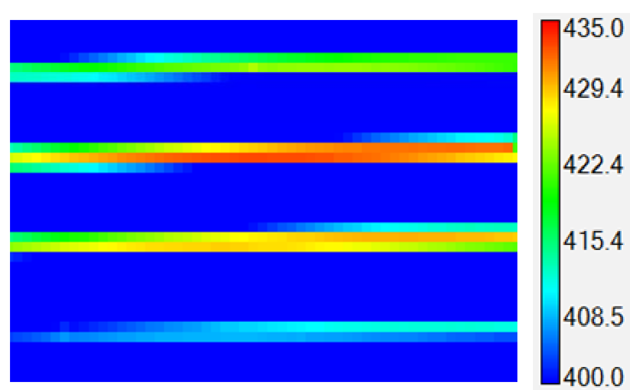

Figure 10: Magnified view of the boxed area in Fig. 7c with a different temperature color range to show the spatial resolution of the infrared thermometry. Each pixel represents 25 μm by μm. When a pixel is not completely on the actuator leg, the temperature is not accurate.

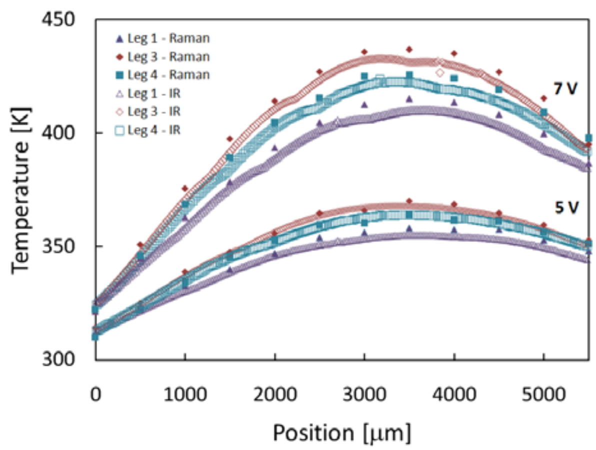

Figure 11: Raman (filled symbols) and IR (open symbols) temperature measurements made at 5V and 7V on the thermal microactuator legs from the anchor (position-0 µm) to the shuttle (position-5500 µm).

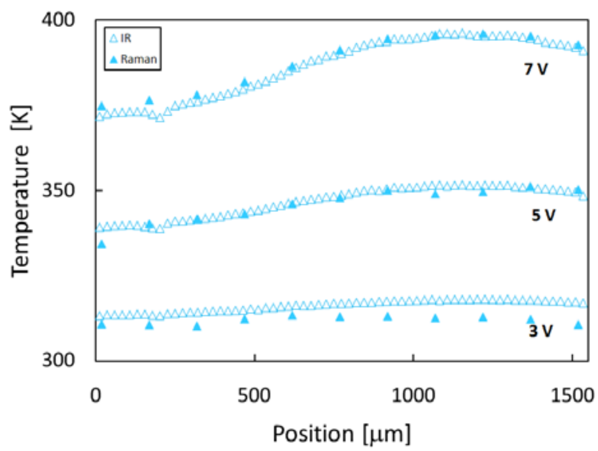

Figure 12: Raman (filled triangles) and IR (open triangles) temperature measurements made at 3V, 5V, and 7V along the centerline of the thermal microactuator shuttle.

The width of the image of beam is about 55 µm corresponding to only two pixels across the width, which is barely enough to make measurement at these thin legs as seen in Fig. 10. Thus, the temperatures across the width of an actuator leg are not plotted for IR as was done for the Raman thermometry in Fig. 5. The pixels at the edge do not provide an accurate temperature measurement, which may result in the waviness of temperature profiles especially at high excitation voltages.

For the shuttle, the temperature profiles of three lines (left edge, center and right edge) are plotted in Fig. 9. The hottest region of the shuttle is at the location where Leg 3 intersects. The shuttle is about 100 µm wide. The temperature profiles for the left edge, center, and right edge are very similar. The edge effect is clear displayed on right edge line at 7 V from 300 to 700 µm. The dip in the temperature line at 200 µm corresponds to a metal line on the shuttle for which the emissivity calibration based on the silicon surface is invalid.

The Raman and infrared measurements are compared directly along Legs 1, 3, and 4 at 5V and 7V in Fig. 11 and along the center of the shuttle in Fig. 12. The Raman data is graphed with filled symbols and the infrared data with open symbols. The Raman and infrared thermometry measurements agree very well. The peak temperature on SOI four-beam thermal microactuators operated in air is located at 60-65% of the distance from the anchor to the shuttle. Also, the inner microactuator beams, Legs 2 and 3, reach higher temperatures than the outer beams, Legs 1 and 4. At 7 V, the peak temperature is 437 and 433 K from Raman and infrared thermometry, respectively. Similarly, the results of shuttle temperature from both techniques are consistent. The peak temperature is 396 K, Raman, and 397 K, IR, at 7V.

Figures 11 and 12 also reveal the strengths and weaknesses of the two techniques. IR thermometry collects a data point per pixel which for the system used is 25 µm by 25 µm, and the spatial extent of a Raman data point is 1.7 µm. Since the IR system collects a full field image and the Raman system needs to scan each location, there are many more data points for the IR measurements along the microactuator legs and shuttle than Raman measurements. However, the Raman system has the resolution to obtain temperature measurements across the width of a microactuator leg, and there are not sufficient pixels across the leg width for the IR system to make multiple temperature measurements. Also, the presence of the metal line on the shuttle impacts the IR thermometry; whereas, metal patterning on the surface is easily avoided when performing Raman measurements.

CONCLUSIONS

This paper reports the temperature measurements on bent-beam thermal microactuators with four legs fabricated using silicon on insulator (SOI) technology. Raman and infrared temperature measurements are reported for a 125 µm thick thermal microactuator with legs 50 µm wide and 5500 µm long from the anchor to the shuttle at voltages ranging from 3V to 9V. Both measurement techniques reveal that the maximum temperature along the thermal microactuator legs are 60-65% of the distance from the anchor to the shuttle and that the inner microactuator beams, legs, achieve higher temperatures than the outer ones. Measurements along the shuttle are also reported using both techniques. The results of these two techniques are consistent qualitatively and quantitatively for the tested conditions. Raman and infrared thermometry are complementary techniques for microsystems when using Raman thermometry to validate the IR calibration and for high spatial resolution measurements and using IR thermometry to obtain full field measurements with faster data collection times.

ACKNOWLEDGEMENTS

Sandia National Laboratories is a multi-program laboratory operated by Sandia Corporation, a wholly owned subsidiary of Lockheed Martin Corporation, for the U.S. Department of Energy's National Nuclear Security Administration under contract DE-AC04-94AL85000. The authors acknowledge Randy Shul for thermal microactuator fabrication, Katie Francis and Ernie Garcia for supplying the thermal microactuators to test, and Allen Gorby for Raman thermometry experimental support.

NOMENCLATURE

e	emissivity
T	Temperature, K

Greek Symbols

Ω	center frequency of Raman peak, cm^{-1}
Ω_o	initial center frequency of Raman peak, cm^{-1}

REFERENCES

1. Skinner, J. L., Dentinger, P. M., Strong, F. W., and Gianoulakis, S. E., 2008, "Low-Power Electrothermal Actuation for Microelectromechanical Systems," *Journal of Micro/Nanolithography, MEMS, and MOEMS*, **7** (4), Article Number 043025, 7 pp.
2. Cahill, D. G., Goodson, K., and Majumdar, A., 2002, "Thermometry and Thermal Transport in Micro/Nanoscale Solid-State Devices and Structures," *Journal of Heat Transfer*, **124** (2), pp. 223-241.
3. Beechem, T., and Graham, S., 2008, "Temperature Measurement of Microdevices using Thermoreflectance and Raman Thermometry," in *BioNanoFluidic MEMS*, P. J. Hesketh, ed., Springer, New York, New York, pp. 153-174.
4. Zhang, Z. M., 2000, "Surface Temperature Measurement Using Optical Techniques," in *Annual Review of Heat Transfer*, C.-L. Tien, ed., Begell House, New York, New York, pp. 351-411.
5. Enikov, E. T., Kedar, S. S., and Lazarov, K. V., 2005, "Analytical Model for Analysis and Design of V-Shaped Thermal Microactuators," *Journal of Microelectromechanical Systems*, **14** (4) pp. 788-798.
6. Chu, L. L., Que, L., Oliver, A. D., and Gianchandani, Y. B., 2006, "Lifetime Studies of Electrothermal Bent-Beam Actuators in Single-Crystal Silicon and Polysilicon," *Journal of Microelectromechanical Systems*, **15** (3) pp. 498-506.
7. Kearney, S. P., Phinney, L. M., and Baker, M. S., 2006, "Spatially Resolved Temperature Mapping of Electrothermal Actuators by Surface Raman Scattering," *Journal of Microelectromechanical Systems*, **15** (2) pp. 314-321.
8. Phinney, L. M., Serrano, J. R., Piekos, E. S., Torczynski, J. R., Gallis, M. A., and Gorby, A. D., 2010, "Raman Thermometry Measurements and Thermal Simulations for MEMS Bridges at Pressures from 0.05 Torr to 625 Torr," *Journal of Heat Transfer*, Vol. 132, No. 7, Article ID 072402, 9 pp.
9. Serrano, J. R., Phinney, L. M., and Kearney, S. P., 2006, "Micro-Raman Thermometry of Thermal Flexure Actuators," *Journal of Micromechanics and Microengineering*, **16** (7) pp. 1128-1134.
10. Machiraju, H., Infantolino, B., Sammakia, B., and Deeds, M., 2007, "Thermal Analysis of MEMS Actuator Performance," *Proceedings of the 2007 ASME International Mechanical Engineering Congress and Exposition*, Paper No. IMECE2007-43475, 6 pp.
11. Cochran, K. R., Fan, L., and DeVoe, D. L., 2004, "Moving Reflector Type Micro Optical Switch for High-Power Transfer in a MEMS-Based Safety and Arming System," *Journal of Micromechanics and Microengineering*, **14** (1) pp. 138-146.
12. Sassen, W. P., Henneken, V. A., Tichem, M., and Sarro, P. M., 2008, "An Improved In-Plane Thermal Folded V-Beam Actuator for Optical Fibre Alignment," *Journal of Micromechanics and Microengineering*, **18** (1) Article No. 075033, 9 pp.
13. Bergna, S., Gorman, J. J., and Dagalakis, N. G., 2005, "Design and Modeling of Thermally Actuated MEMS Nanopositioners," *Proceedings of the 2005 ASME International Mechanical Engineering Congress and Exposition*, Paper No. IMECE2005-82158, 8 pp.
14. Baker, M. S., Plass, R. A., Headley, T. J., and Walraven, J. A., 2004 "Final Report: Compliant Thermomechanical MEMS Actuators LDRD #52553," Sandia report SAND2004-6635, Sandia National Laboratories, Albuquerque, NM.
15. Wong, C. C., and Phinney, L. M., 2007 "Computational Analysis of Responses of Micro Electro-Thermal Actuators," *Proceedings of the 2007 ASME International Mechanical Engineering Congress and Exposition*, Paper No. IMECE2007-41462, 9 pp.
16. Hickey, R., Sameoto, D., Hubbard, T., and Kujath, M., 2003, "Time and Frequency Response of Two-Arm Micromachined Thermal Actuators," *Journal of Micromechanics and Microengineering*, **13** (1) pp. 40-46.
17. Lott, C. D., McLain, T. W., Harb, J. N., and Howell, L. L., 2002, "Modeling the Thermal Behavior of a Surface-Micromachined Linear-Displacement Thermomechanical Microactuator," *Sensors and Actuators A*, **101** (1-2) pp. 239-250.
18. Milanović, V., 2004, "Multilevel Beam SOI-MEMS Fabrication and Applications," *Journal of Microelectromechanical Systems*, **13** (1) pp. 19-30.
19. Beechem, T., Graham, S., Kearney, S. P., Phinney, L. M., and Serrano, J. R., 2007, "Simultaneous Mapping of Temperature and Stress in Microdevices Using Micro-Raman Spectroscopy," *Review of Scientific Instruments*, **78**(6), Paper No. 061301, pp. 1-9.
20. Sato. T., 1967 "Spectral Emissivity of Silicon," *Japanese Journal of Applied Physics*, 6 (3) pp. 339-347.